Applied Physics B (2022) 128:15
https://doi.org/10.1007/s00340-021-07745-z

Applied Physics B
Lasers and Optics

Investigation of the opto-thermo-mechanical properties of antimicrobial PET/TiO_2 fiber using the transport of intensity equation technique

G. M. Abo-Lila[1] · T. Z. N. Sokkar[1] · E. A. Seisa[1] · E. Z. Omar[1,2]

Received: 3 November 2021 / Accepted: 20 December 2021 / Published online: 6 January 2022

Abstract

The transport of intensity equation (TIE) technique is used to investigate the effect of stretching and annealing conditions on the optical features and antimicrobial activity of polyethylene terephthalate (PET) fibers treated with TiO_2 nanoparticles. The main core of this paper gets the most preferable optical and mechanical properties for PET/TiO_2 fiber which maintains its antibacterial activity. The variation of the refractive index of untreated PET/TiO_2 fiber along its axis is studied. The computed tomography technique is used to investigate the morphology of the tested fiber and the distribution of TiO_2 nanoparticles inside the fiber. The effect of stretching on the refractive index and the density of TiO_2 nanoparticles of drawn PET/TiO_2 fibers are carried out. The antimicrobial activity of the PET/TiO_2 fibers are evaluated before and after stretching. The PET/TiO_2 fibers are annealed at different temperatures and durations. The influence of annealing on the variation of the refractive index of PET/TiO_2 fiber along its axis and the distribution of TiO_2 is investigated.

1 Introduction

In the shadow of the Covid-19 pandemic and the presence of many harmful microorganisms that negatively affect the human health, the antimicrobial fibers become a significant element to avoid and confront these epidemics [1, 2]. The antimicrobial fibers are a mixture between traditional fiber materials and antimicrobial agents [3]. These fibers have the ability to inhibit the growth of the microorganisms or kill them on their surfaces [3–5]. The most common antimicrobial agents, which are used in the manufacture of antimicrobial fibers, include silver (Ag), cooper oxide (CuO), titanium dioxide (TiO_2), zinc oxide (ZnO), and others [6–8]. The mechanism of incorporating the antimicrobial agent into fiber matrix relies on the fiber kind and its composition and morphology [3, 5]. In the majority cases of polymer fibers , the antimicrobial agents are chemically bonded to the fiber [6, 7].

✉ E. Z. Omar
emam11088@gmail.com

1 Physics Department, Faculty of Science, Mansoura University, Mansoura, Egypt

2 Physics Department, Faculty of Science, New Mansoura University, New Mansoura City, Egypt

The antimicrobial fibers play an important role in medical field in which fabrics contaminated with microbes that medical staff and patients wear in hospitals are considered the main source of infection [2, 8]. So, towels, masks, surgical gown, blanket materials, and pillowcases used in hospitals should be manufactured from fibers having antimicrobial features. Also, the antimicrobial fibers have many applications in industry and everyday uses. These applications include air filters, food packaging, water purification devices, sport equipment and clothes, automotive textiles, mechanical and thermal protection systems [1, 8]. Due to the extreme importance of antimicrobial fibers and their various applications in different fields, the investigation of morphology, opto-mechanical and opto-thermal properties of these materials becomes a serious task to improve their features.

Transport of intensity equation (TIE) technique is considered one of the simplest and most accurate techniques to investigate the opto-mechincal and opto-thermal properties of tested fibers [9, 10]. Many authors have used the TIE technique to investigate the structural and optical properties of fibrous materials with high degree of accuracy [10–12]. This technique has the ability to demodulate the phase map of the tested samples via linking the variation in axial intensity for optical field with phase [9]. To demodulate the phase map using this technique, three intensity images for the tested fiber are needed. One of them is captured at the focus plane and the other two intensity images are captured at defined defocus planes [11, 12]. The demodulated phase object via the TIE technique has worthy information such as surface profile, refractive index, degree of crystallinity, and polarizability [10, 13]. The TIE technique has many unique advantages such as stability in measurements, simple optical setup (does not need reference beam), produce directly absolute phase map, capabilities to work with partially coherent source, and does not need iterations (simple calculations) [10, 12, 14].

Computed tomography (CT) is considered as an accurate technique to investigate the morphology and the internal structures of fibrous materials [15, 16]. It has the ability to reconstruct the real 3D shape of tested fibers using sequence images of thin sections [15]. The CT has many applications especially in biology and medicine sciences [17]. CT can be divided into two main processes [18]. The first process is tomographic recoding process. In this process, the TIE technique is utilized to capture several 2D intensity images at different angular orientations about the vertical axis of the tested fiber [17]. The second process is tomographic reconstruction, in which the cross-section of the tested fiber can be reconstructed via one of tomographic reconstruction techniques such as the filtered back-projection algorithm [18].

Generally, most of the undrawn fibrous materials are not satisfactory and possess unfavourable features such as low modulus, high plastic deformability, and low tenacity [19–21]. This is because the random molecular orientation of fiber chains [20]. The mechanical stretching and annealing for fibrous materials are pivotal and important processes in order to improve its physical properties, especially the mechanical features [20, 22]. Several authors have reported that the tensile breaking strength and the molecular orientation chains of fibrous materials increased due to stretch whereas toughness and plasticity of fibrous materials decreased due to stretch [19–22]. Annealing process is also a considerable tool to enhance the mechanical properties of fibrous materials because the viscoelastic behavior of these materials has high sensitivity to annealing process [20, 22]. Increasing the viscoelastic behavior of fibrous materials may increase its performance and lifetime [19, 22].

On the light of the previous mentioned techniques, this research aims to get the optimum optical and structural properties for synthetic PET/TiO_2 fiber while maintaining its antibacterial activity. The stretching and annealing treatments are utilized to improve the optical, mechanical, and antimicrobial properties of PET/TiO_2 fibers . The TIE technique is used to carry out investigation for the variations in the refractive index due to the stretching. The computed tomography technique is used to investigate the morphology of the tested fiber and the distribution of TiO_2 nanoparticles inside the fiber. The antimicrobial activity of the PET/TiO_2 fiberes are evaluated before and after stretching. The effect of annealing on the variation of the refractive index of PET/TiO_2 fiber along its axis and the distribution of TiO_2 are investigated.

2 Theoretical considerations

2.1 Demodulating the phase object using the transport of intensity equation (TIE) technique

The phase of tested fibrous materials can be demodulated via the TIE technique using the following equation [9, 12];

$$\psi(x,y) = \mathfrak{F}^{-1}\left[\frac{1}{k_x^2 + k_y^2}\mathfrak{F}\left(\frac{2\pi}{\lambda g_o}\frac{g_1(x,y;z_0+\Delta z) - g_2(x,y;z_0-\Delta z)}{2\Delta z}\right)\right], \tag{1}$$

where λ is the wavelength of the used light, g_o is the captured intensity image at the focus plane, $g_1(x,y;z_0+\Delta z)\&g_2(x,y;z_0-\Delta z)$ are the captured intensity images at defocus planes up and down, respectively, Δz refers to the separation distance between the two recoding intensity planes, k_x & k_y are the spatial frequencies in Fourier domain, $\mathfrak{F}\&\mathfrak{F}^{-1}$ refers to apply Fourier and inverse Fourier transforms, respectively.

2.2 Refractive index profile

According to the demodulated phase in Eq. (1), the refractive index profile of fibrous material can be calculated using the following equation [23];

$$n(x,y) = \frac{\psi(x,y)\lambda}{2\pi t} + n_L, \tag{2}$$

where t is the thickness of the fiber, and n_L is the refractive index of the immersion liquid.

2.3 Tomographic reconstruction using filtered back-projection algorithm

Using the computed tomography (CT) technique, the recorded intensity image at the focus plane can be modified to include fiber rotation relative to the direction of measuring beam. So, the intensity image at the focus plane is given by the function $P(\alpha_o, w, z)$ corresponding to the angular position ($\alpha = \alpha_o$). The 1D $P(\alpha_o, w, z_o)$ is called a projection P. Single cross-section $\varphi(x, y, z_o)$ can be extracted using the series of projections $P(\alpha_i, w, z_o)$, where the typical range of

α_i is 1°–179° with step 1°. To perform this task, the filtered back-projection fundamental is used as shown in the following equation [16, 18]:

$$\Delta\varphi\left(x,y,z_o\right)=\int_0^{\pi}\int_{-\infty}^{\infty}S\left(\alpha,\omega,z_o\right)|\omega|\exp\left(j2\pi w\omega\right)d\omega d\alpha\,, \quad (3)$$

where the function $S\left(\alpha,\omega,z_o\right)$ can be defined as follows:

$$S\left(\alpha,\omega,z_o\right)=\int_{-\infty}^{\infty}P\left(\alpha,w,z_o\right)\exp\left(-j2\pi w\omega\right)d\omega\,, \quad (4)$$

where ω is the spatial frequency of the function $P(\alpha, w, z_0)$. By the same way, the next cross-sections $\varphi(x,y,z_o+1,2,3,\dots Z)$ are obtained sequentially from the sets of projection $P(\alpha,w,+1,2,3,\dots Z)$, where Z is the number of recorded intensity images.

3 Materials

The samples used in this work are polyethylene terephthalate (PET) fiber which was obtained from PET chips supplied by FIBERTEX Company and (PET) fiber treated with TiO_2 nanoparticles [24]. The manufacture of the fiber is carried out at spinning line located in FIBERTEX Company, Abo-Rawash, Egypt [24]. The percentage of TiO_2 added to PET is 1.0% on the weight of polymer chips. The melting point (T_m) of the PET materials ranged from 250 to 260 °C and its glass transition temperature (T_g) is 70 °C [24].

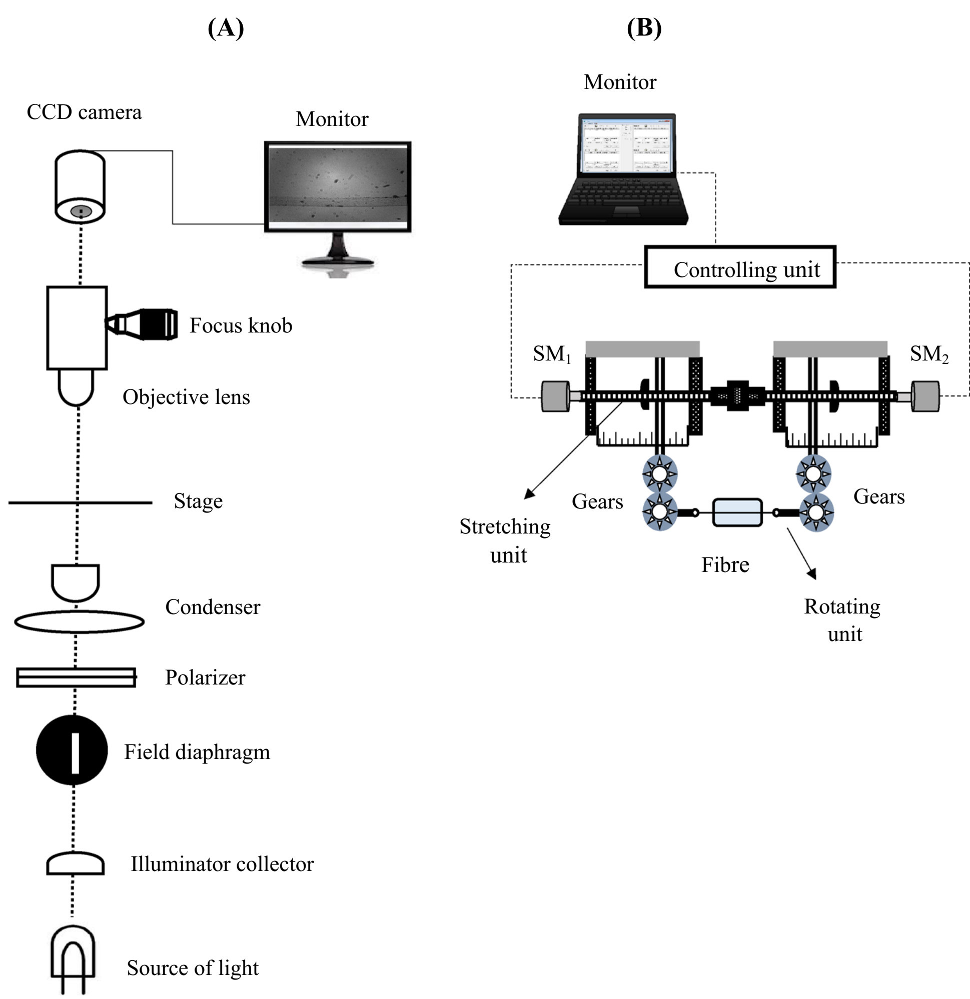

Fig. 1 **A** Schematic diagram for the optical system setup of TIE technique. **B** Stretching and rotation unit

4 Experimental techniques

Here, the TIE technique is preferred over the optical interferometric techniques to perform the current study. This is because the nanoparticles present in the tested samples might cover the shifts of the interference fringes, which makes it difficult to extract their phase maps. The optical system of the modified TIE technique [12] is utilized to investigate the optical properties of the tested samples as shown in Fig. 1A. In this optical system, the polarizer is used to adjust the angle between the direction of the light wave vibration and the fiber's axis, the focus knob is used to generate intensity images at various focus planes, and the charge coupled device (CCD) camera is used to acquire the intensity images. The wavelength of the used monochromatic light is 546 nm. The microscope stage in this optical system is movable to change the position of tested sample each 1 mm ± 0.05 mm.

The optical system of the modified TIE technique is fitted with stretching and rotation unit as shown in Fig. 1B. This unit is used to draw the tested samples at a defined draw ratio and capture intensity images at different angular orientations about the vertical axis of the tested sample. The stretching and rotation unit includes two stepper motors (SM_1 & SM_2). Only, the SM_1 is used to stretch the fiber sample. Both SM_1 & SM_2 are utilized to rotate the fiber in steps each 10°. A Matlab software is designed to automatically control the stretching and the rotation values.

5 Results and discussions

5.1 Evaluating antimicrobial activity of the PET/TiO_2 fiber using the shaking flask method

In this work, the shake flask method [25–27] is used to evaluate the antibacterial activity of the PET/TiO_2 fibers by investigating the rate of reduction (Rp %) in the number of bacteria [26]. This method is selective to observer growth inhibition by the fibrous (fabrics) materials [27]. In this method, 0.4 g of tested samples are sufficient to inhabit the bacterial growth. Here, 0.4 g of PET/TiO_2 and 0.4 g of blank PET fibers are placed in contact with 20 ml of sterile saline in two individual shaking flasks. Then, the PET/TiO_2 and blank PET fibers are inoculated with 1 ml of bacterial inoculums and the two flasks are incubated in a rotary shaking incubator at 37 °C for 24 ± 1 h. The result for this test is taken as optical density (O. D) at which absorption (turbidity) checked at 600 nm is given in Table 1. In this table, the reduction percentage of *Bacillus subtilis* growth is 80.5% that indicates the antibacterial activity for PET/TiO_2 fiber.

Table 1 Results of shaking flask test for untreated of PET and PET/TiO_2 fiber in terms of percentage growth reduction

Test microorganism	O.D after 24 h. 600 nm		Reduction (Rp) % for PET/TiO_2 fibers
	Blank PET fiber	PET/TiO_2 fiber	
Bacillus subtilis	0.360	0.070	80.5%

5.2 Investigation of the variation of the refractive index of antibacterial PET/TiO_2 fiber along the fiber axis using the TIE technique

To investigate the influence of the TiO_2 particles on the PET samples, the TIE technique is used to explore the variation of the refractive index of PET/TiO_2 fiber along its axis. Here, a mono filament of PET/TiO_2 fiber is fixed on a glass slide and immersed in liquid (1-Bromonaphthalene) of refractive index 1.65 at room temperature and then transferred to the microscope stage in Fig. 1A. In this optical system, the microscope stage is utilized to shift the position of the PET/TiO_2 fiber each 1 mm ± 0.05 mm along its axis. Also, the polarizer is adjusted to allow the light waves to vibrate in parallel direction with respect to the fiber axis.

For each position, three two-dimensional intensity images for the PET/TiO_2 fiber separated via 50 microns from focus at the parallel (∥) polarization direction are captured using the optical system of TIE technique as shown in Fig. 2. Using Eq. (1), the phase map of PET/TiO_2 fiber at each position is extracted as shown in Fig. 3A. Using the extracted phase maps in Fig. 3A, the 3D visualization of refractive index for PET/TiO_2 fiber at each position is calculated using Eq. (2) and the results are shown in Fig. 4. In this figure, it is obvious that the refractive index values change from one segment to another along the fiber for each fibre position. For example, the segment R4 in the 3D visualization of refractive index at position $d = 1$ mm has the higher refractive index value compared to the segments R1, R2, R3. With the same manner, segment R1 in the 3D visualization of refractive index at position $d = 5$ mm has the higher refractive index value compared to segment R2 and so on and so forth for the other fiber positions.

To interpret and understand the reason for these significant changes in the refractive index values, the filled contour method is used. This method is a topographical technique for representing a three-dimensional surface via plotting z slices (contours lines) on a flat two-dimensional surface [28] in which, the regions between lines are filled with colors. Figure 3B shows the filled contour plots for the extracted

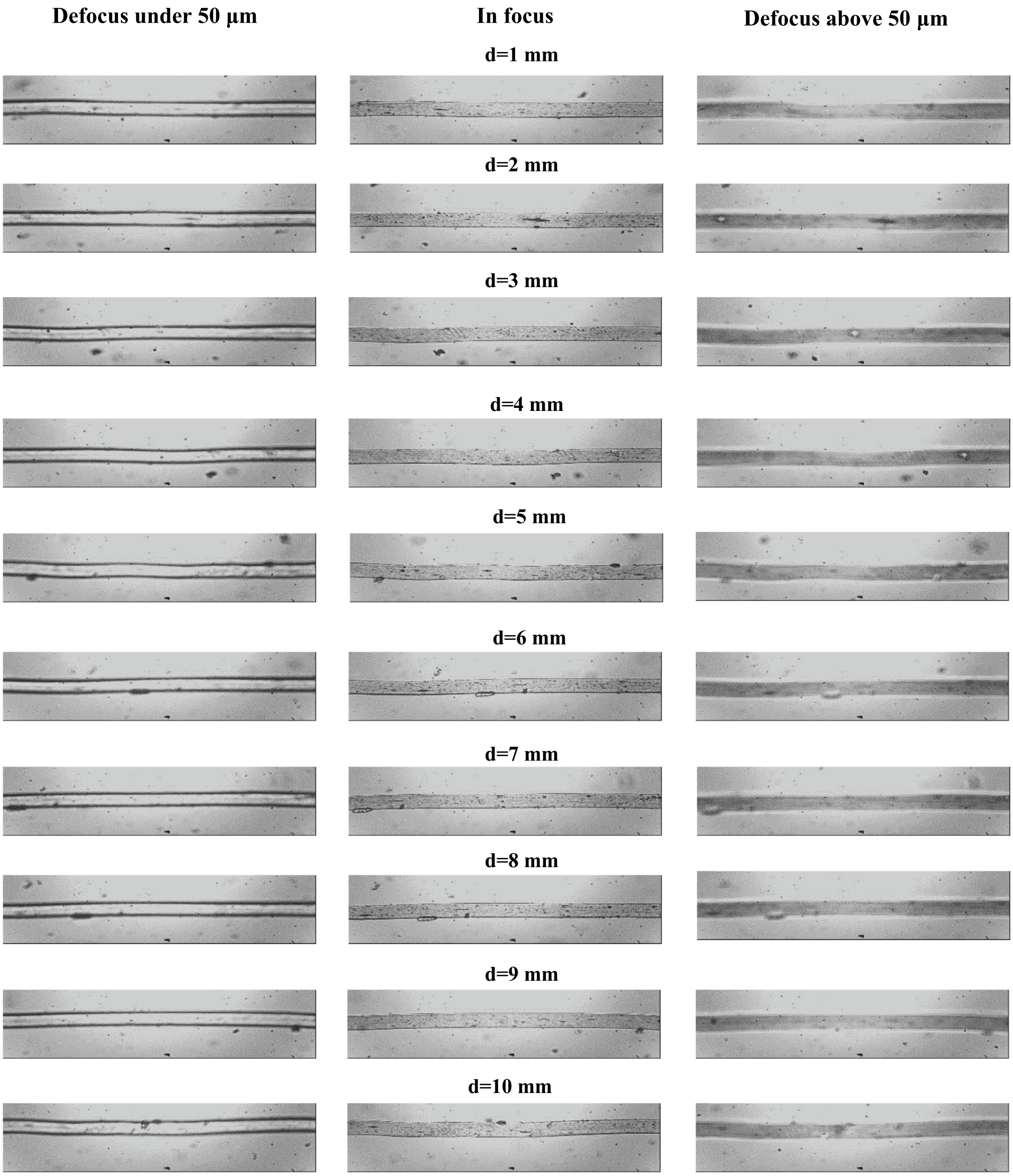

Fig. 2 Recorded three two-dimensional intensity images for the PET/TiO_2 fiber separated via 50 microns from focus at the parallel (∥) polarization direction at different position along the fiber

phase maps of PET/TiO_2 fiber in Fig. 3A. In this figure, each degree of color refers to a certain segment along the fibre that has the same composition, concentration, and features. According to the given color map above the filled contour plots of phase maps, it is obvious that each segment along the fibre axis has different color or in other words has different optical phase values, where the higher optical phase (deeper red color) segments have different composition and features compared to the lower optical phase (cooler blue color) segments.

Here, we considered that the deeper red color segments have higher concentration and density of TiO_2 nanoparticles compared to the cooler color segment. This is because TiO_2 nanoparticles have high refractive index value (high optical

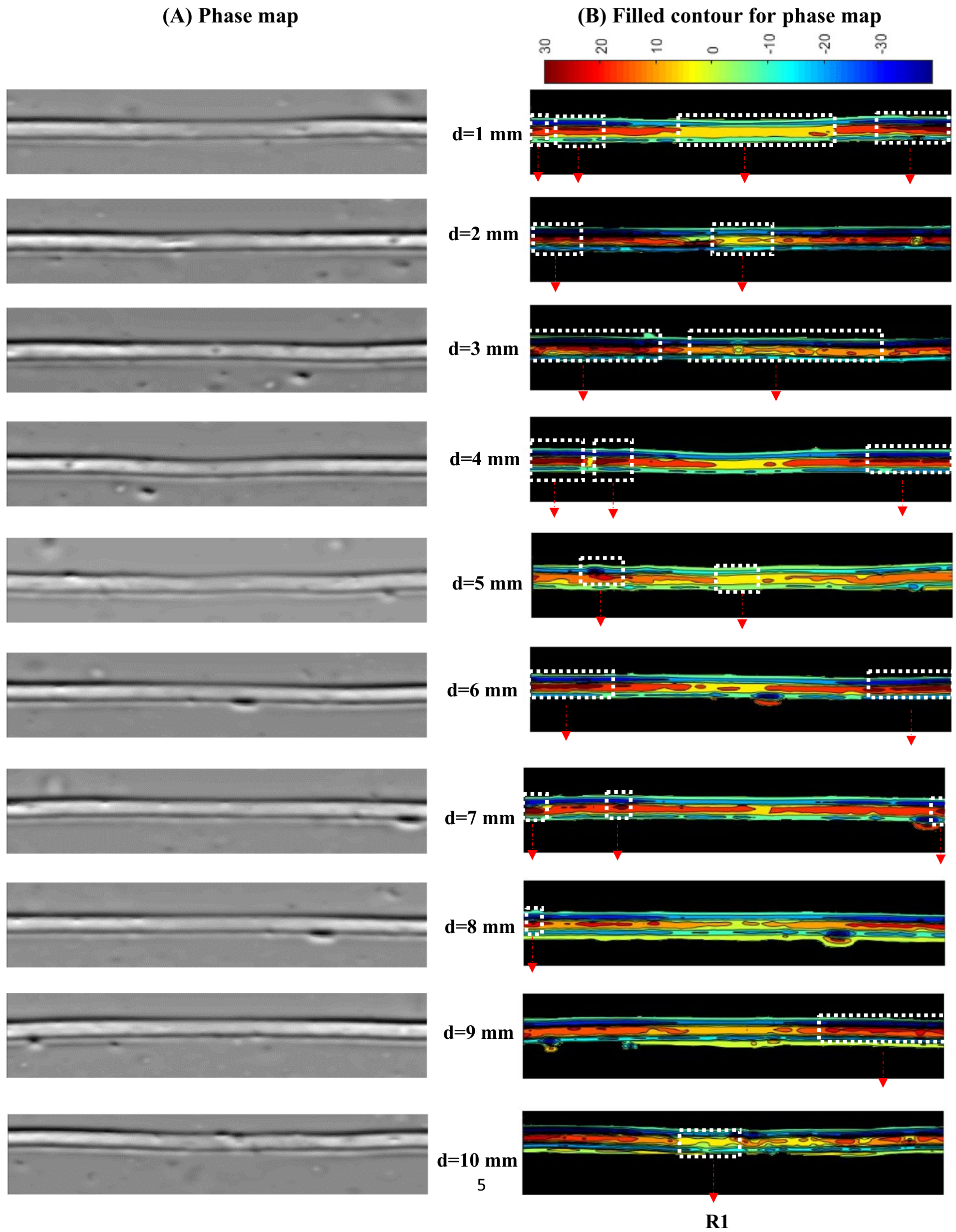

Fig. 3 **A**, **B** Demodulated phase map of PET/TiO_2 fiber at different position along the fiber and their filled contour plots, respectively

phase) compared to refractive index of blank PET material. From the given filled contour plots of phase maps in Fig. 3B at fiber position $d = 1$ mm, it is clear that segment R4 has the deeper red color (high concentration of TiO_2 nanoparticles) compared to the other segments. In the same manner, the segment R1 in its filled contour plot at d = 5 mm has the deeper red color compared to the R2 segment. This explains why the refractive indices of segment R4 at $d = 1$ mm and segment R1 at $d = 5$ mm have the higher values compared to their other segments. The mean refractive index of PET/TiO_2 fiber which is calculated from taking the average of refractive index values for the center line along the fiber at each position is given in Fig. 5. From this figure, it is noticed that there are large variations in the refractive index values along the fiber. From above, one concludes that the distributions and concentrations of TiO_2 nanoparticles is random along the fiber and this considered the main reason for the variation in refractive index values along the fiber. Also, segments containing higher concentrations of TiO_2 nanoparticles (deeper red color) have higher refractive index values.

For confirming that the high refractive indices in some regions of PET/TiO_2 fiber are correlated to high concentration of TiO_2 nanoparticles, the refractive index of the blank PET fiber is determined. Figure 6 shows three recorded

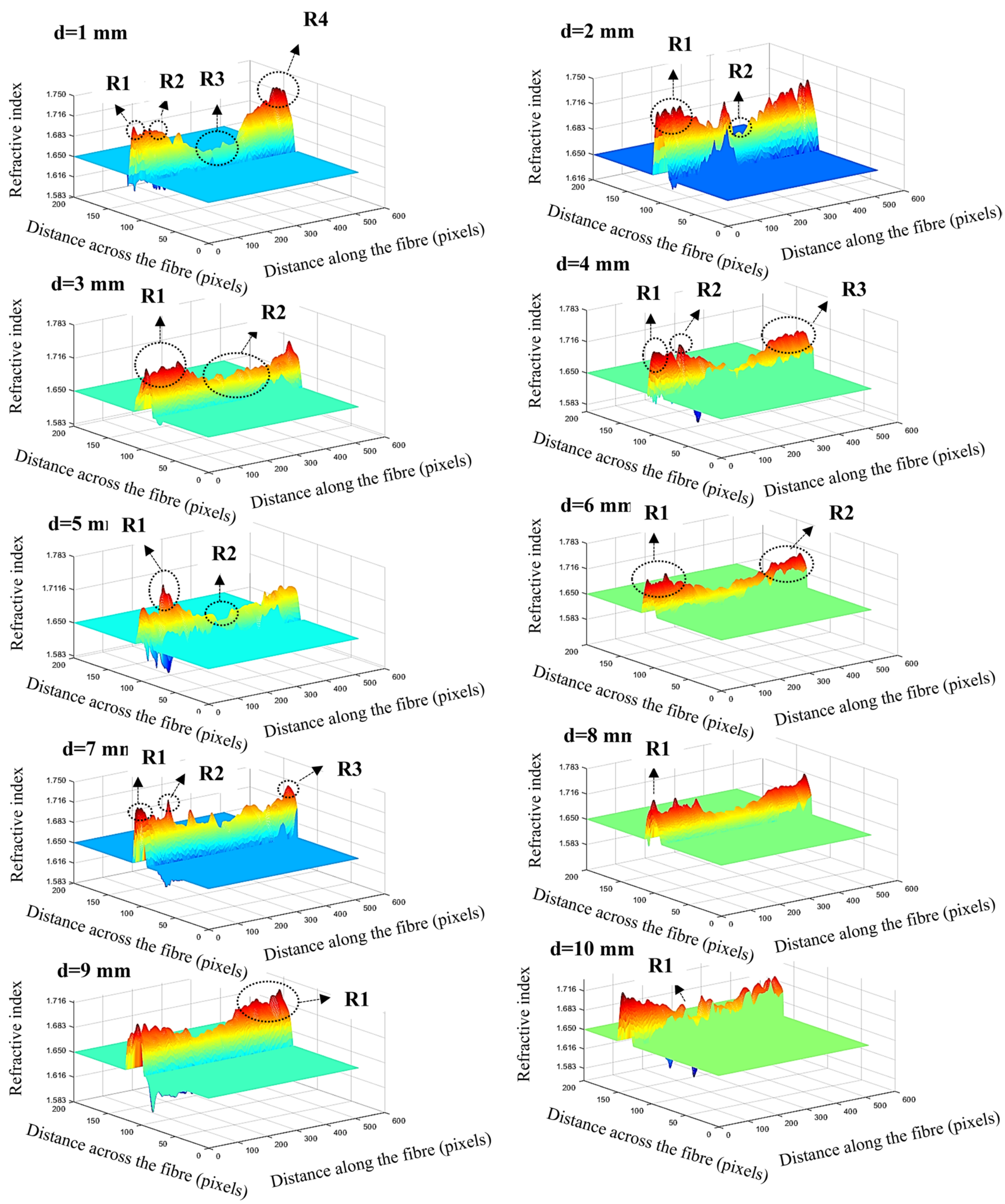

Fig. 4 The 3D visualization of refractive index for PET/TiO_2 fiber at different positions along the fiber

two-dimensional intensity images for blank PET fiber separated via 50 microns from focus at the parallel (∥) polarization. Using Eqs. (1, 2) the phase map and refractive index of blank PET fiber are calculated, respectively. Here, the average refractive index is determined and found to be 1.56. On the other hand, the literatures have reported that TiO_2 nanocomposites have a high refractive index equal to ~ 2.45 [29–31]. Therefore, any region in the PET/TiO_2 fiber have high concentration of TiO_2 nanoparticles compared to the concentration of PET will show relative high refractive index. These results are in good agreement with published data in References [29–31].

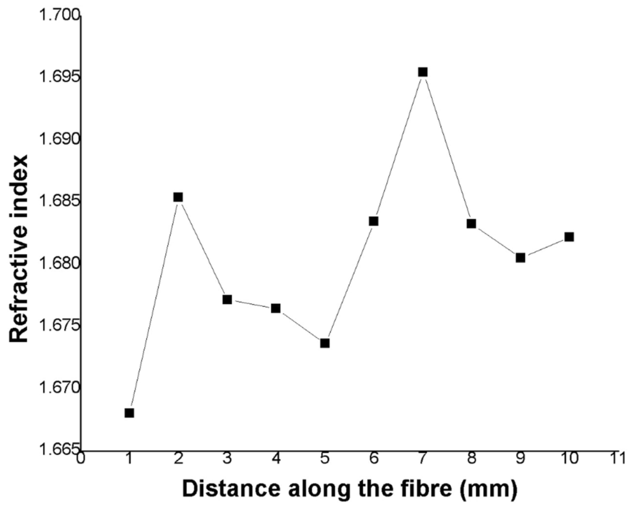

Fig. 5 Relation between the mean refractive index of PET/TiO_2 fiber as a function of fiber position

5.3 Investigation of the morphology and internal structure of PET/TiO_2 fiber by using tomographic transport of intensity equation technique

To cross-check the random distribution of TiO_2 nanoparticles along the PET fiber, the tomographic transport of intensity equation technique is utilized to investigate the morphology and internal structure of PET/TiO_2 fiber. In this experiment, the ends of PET/TiO_2 fiber is fixed between the clamps of the rotating device unit (see Fig. 1B) and immersed in liquid of refractive index 1.65 at room temperature and then they are transferred to the microscope stage in Fig. 1A. Here, signals are sent to the both stepper motors (SM_1 & SM_2) to rotate the PET/TiO_2 fiber at different angular orientations from 1° to 179° with rotation resolution of $10° \pm 0.2°$.

For each angular orientation, three two-dimensional intensity images for the PET/TiO_2 fiber separated via 50 microns from focus are captured using the optical system of TIE technique. Figure 7A shows some of the extracted phase maps using Eq. (1) of the PET/TiO_2 fiber at angular orientations 1°, 30°, 60°, 90°, 120°, and 179°, respectively. The 3D phase $\Delta\varphi(x, y, z_o)$ of PET/TiO_2 fiber is reconstructed via the filtered back-projection technique using Eqs. (3) and (4). Figure 7B(I–IV) shows the 3D visualization of PET/TiO_2 fiber by longitudinal planes at distances 4 µm, 12 µm, 18 µm, and 27 µm, respectively, from the core of the fiber. Also, lateral slices along the PET/TiO_2 fiber at distances 10 µm, 20 µm, 30 µm, 40 µm, 50 µm, and 60 µm are displayed as shown in Fig. 7B(V). These longitudinal and lateral slices clarify the random distribution and concentrations of TiO_2 particles (deeper red color) inside the tested sample. This confirms that the main reason for the variation in refractive index along the fiber in the abovementioned study is the random distribution of TiO_2 particles inside the tested sample.

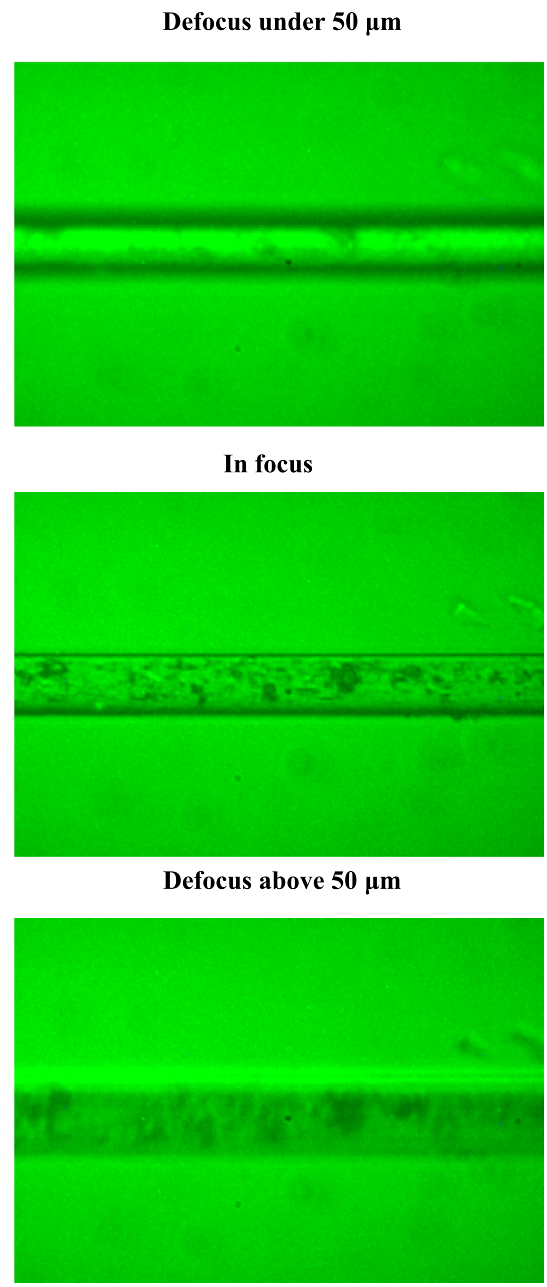

Fig. 6 Recorded three two-dimensional intensity images for blank PET fiber separated via 50 microns from focus at the parallel (||) polarization

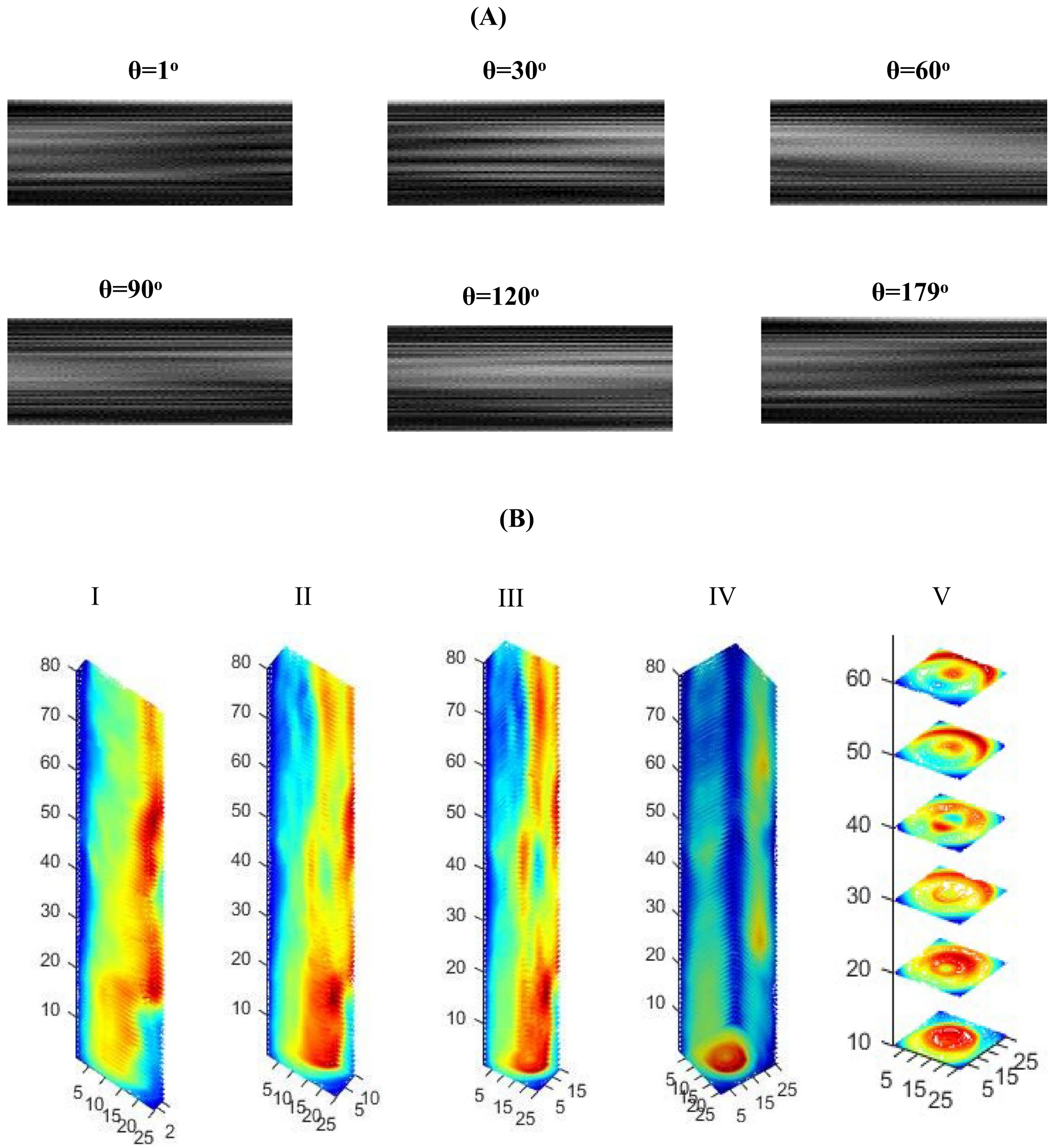

Fig. 7 **A** Extracted phase maps of the PET/TiO_2 fiber at angular orientations 1°, 30°, 60°, 90°, 120°, and 179°, respectively. **B** The 3D visualization of PET/TiO_2 fiber by longitudinal planes at different distances from the core and lateral slices along the PET/TiO_2 fiber, respectively

5.4 Influence of the cold drawing process on the composition and optical properties of PET/TiO_2 fiber

Here, the optical system of the TIE technique in Fig. 1A with aids of mechanical device unit in Fig. 1B are used to perform opto-mechincal study for PET/TiO_2 fiber. In the current study, a mono filament of PET/TiO_2 fiber is fixed between the clamps of the stretching device unit and immersed in liquid of refractive index 1.65 at room temperature and then they are transferred to the microscope stage in optical system of TIE technique. Signals are sent to the stepper motor SM_1 to draw the PET/TiO_2 fiber at different draw ratios. For each draw ratio, three two-dimensional intensity images for the PET/TiO_2 fiber separated via 50 microns from focus at the parallel (ǁ) polarization direction are recorded using the optical system of

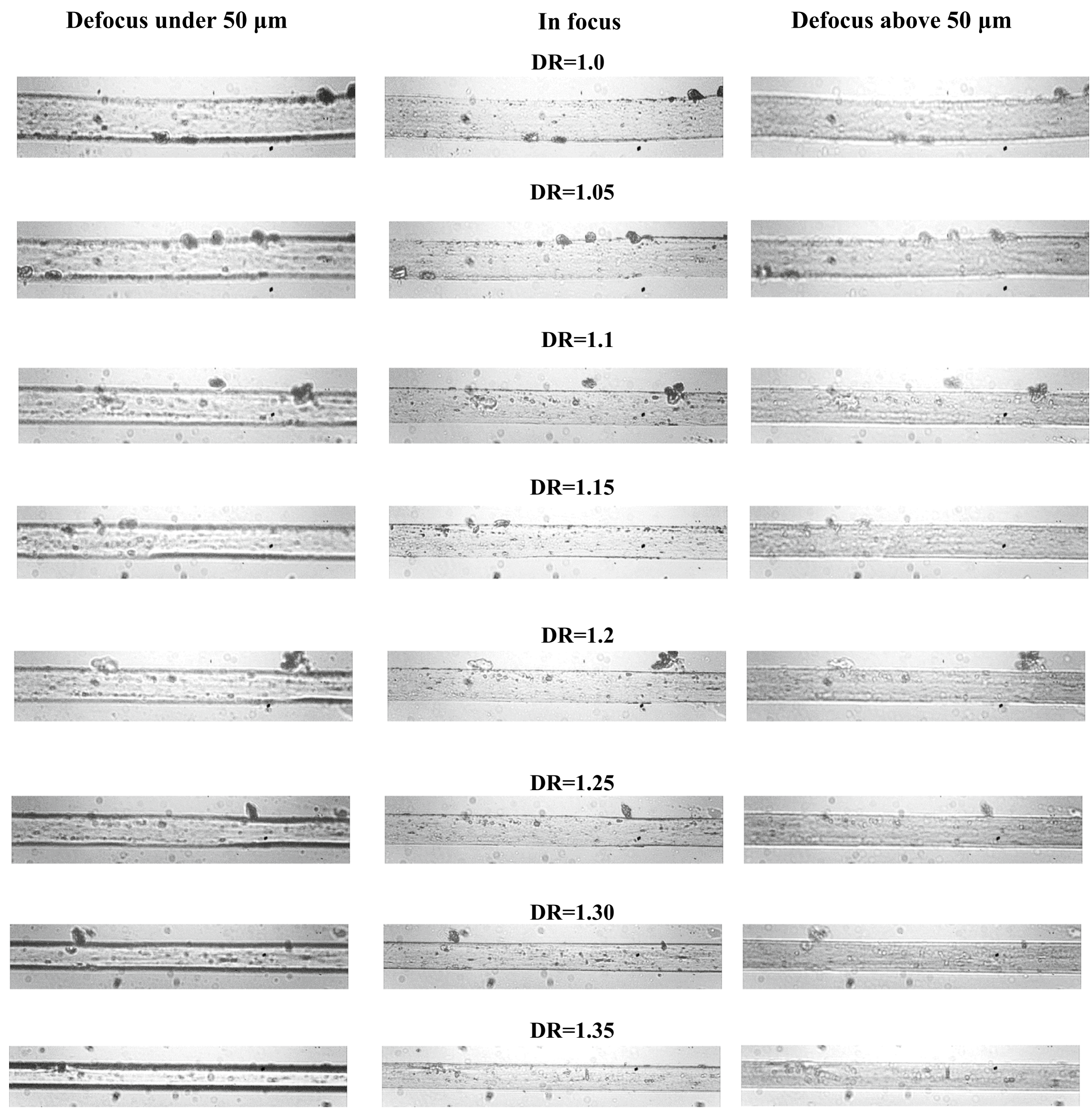

Fig. 8 Recorded three two-dimensional intensity images for the PET/TiO_2 fiber separated via 50 microns from focus at the parallel (∥) polarization direction at different draw ratios

TIE technique as shown in Fig. 8. The phase map of PET/TiO_2 fiber at each draw ratio is retrieved and the results are shown in Fig. 9A. Also, their filled contour plots are shown in Fig. 9B.

According to the extracted phase maps in Fig. 9A, the 3D visualization of refractive index for PET/TiO_2 fiber at each draw ratio is calculated as shown in Fig. 10. Also, the mean refractive index of PET/TiO_2 fiber is plotted as a function of draw ratio as shown in Fig. 11. These figures clarify that the refractive index decreases with increases the draw ratio. To interpret this result, the filled contour plots in Fig. 9B will be used. In this figure, it is obvious that the presence and concentration of TiO_2 nanoparticles (deeper red color) decrease with the increase the draw ratio value. Hence, the refractive indices of PET/TiO_2 fiber decreases with increases the draw ratio value due to decreasing the concentration and size of TiO_2 nanoparticles. The main reason for decreasing the concentration and size of TiO_2 nanoparticles may be attributed to the breakup of the aggregates of TiO_2 nanoparticles into much smaller particles (like the glass smash) and redistributed along the fiber due to the drawing process and these results are in good agreement with results that obtained by Vermillac et al. in Ref [32].

The antibacterial activity of the stretched PET/TiO_2 fiber at DR = 1.3 is evaluated using the shaking flask method and

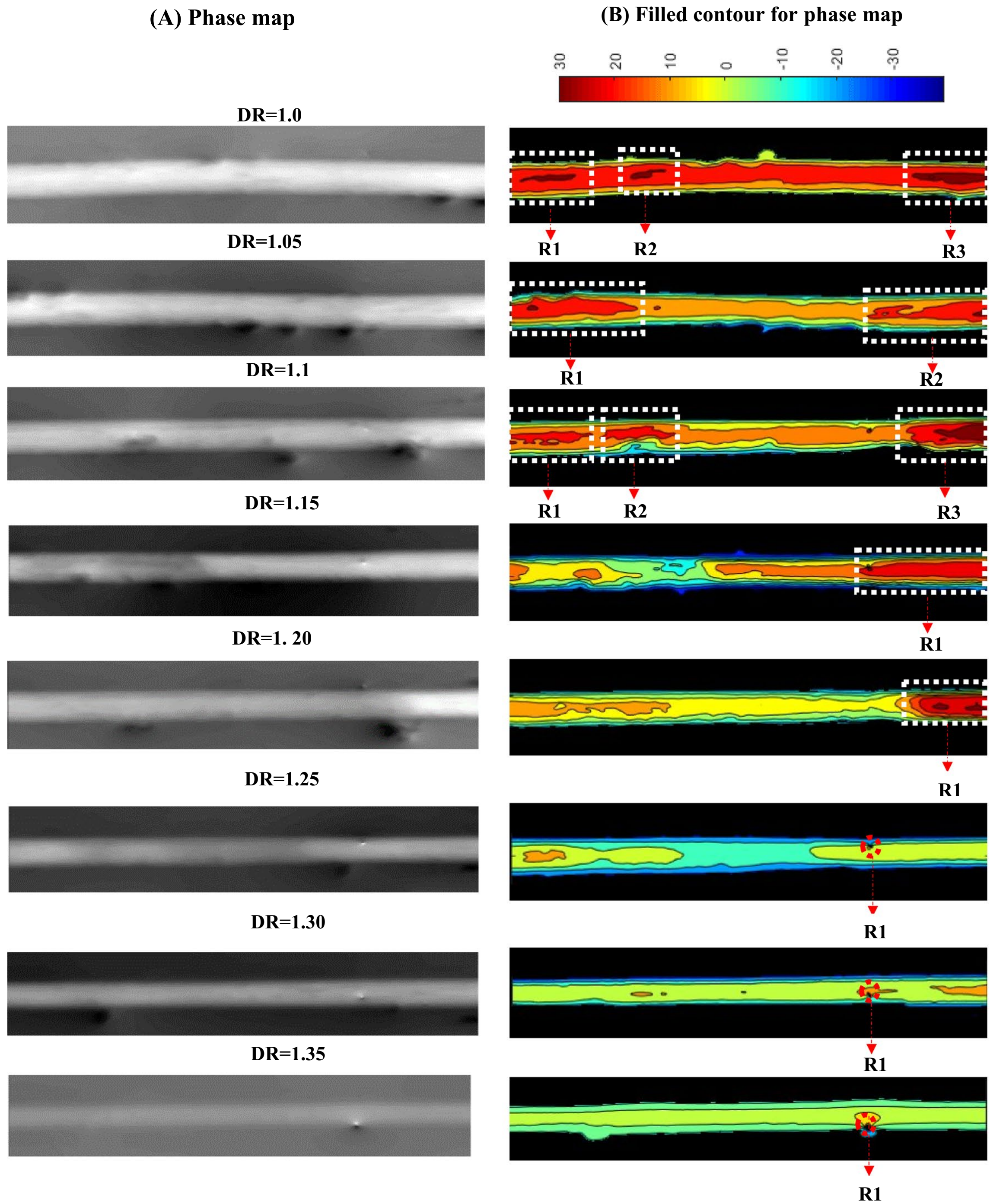

Fig. 9 **A**, **B** Demodulated phase map of PET/TiO_2 fiber at different draw ratios and their filled contour plots, respectively

the results are shown in Table 2. This table clarifies that the reduction percentage increased to reach 91.6% comparing to undrawn fiber (80.5%) in Table 1. This is because the drawn process leads to smash nanoparticle groping that increase surface to volume ratio. Also, the small size of the nanoparticles' aggregation (see region R1 at DR = 1.25, 1.3 and 1.35 in Fig. 10) helps to increase the antibacterial activity and these results are in good agreement with results obtained by Yetisen et al. and Vermillac et al. in Refs [6, 32].

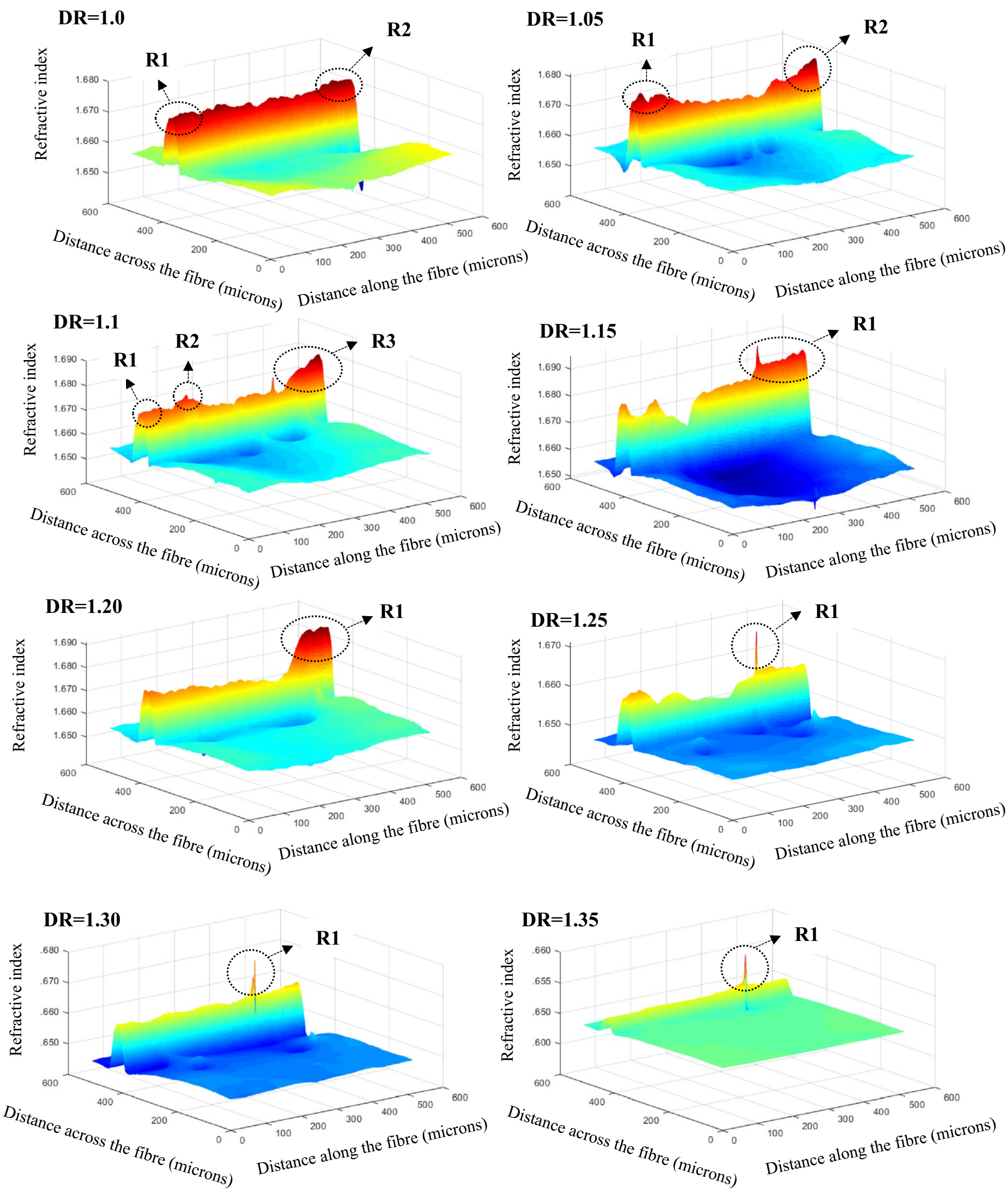

Fig. 10 The 3D visualization of refractive index for stretched PET/TiO_2 fiber at different draw ratios

5.5 Effect of annealing treatment on the optical properties, mechanical properties, and antibacterial activity of PET/TiO_2 fiber

Here, an electric oven is used for annealing undrawn PET/TiO_2 fibers with free ends at the following temperatures: 70 °C, 80 °C, 90 °C, 100 °C, 110 °C, and 120 °C with accuracy ± 3 °C. Four annealing durations: 30 min, 60 min, 90 min, and 120 min are performed for each annealing temperature. These temperatures are selected according to the T_g and the T_m of the tested fiber. Also, the selection of annealed temperatures should be in the range that maintains the antimicrobial activity of PET/TiO_2 fiber. Previous studies reported that the TiO_2 nanoparticles treated at 120 °C showed a maximum antibacterial activity while those treated at temperatures higher than 120 °C showed no activity against the examined selected bacteria [33]. After the heat setting, the annealed PET/TiO_2 fibers are allowed to cool away from the oven to the ambient temperature.

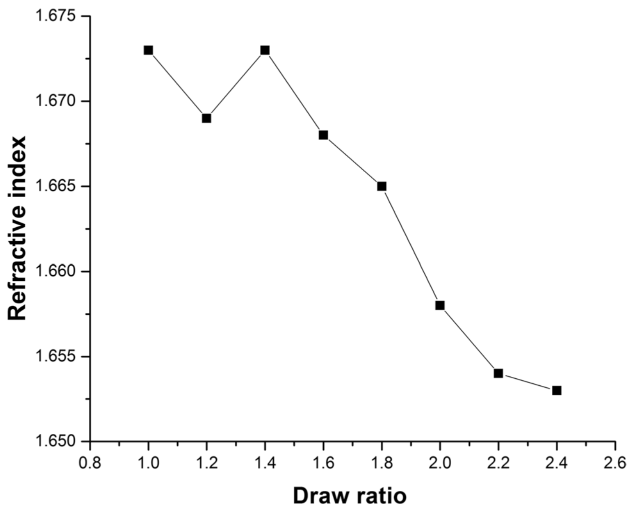

Fig. 11 Relation between the mean refractive index of PET/TiO_2 fiber as a function of draw ratio

Table 2 The reduction percentage in the growth of *Bacillus subtilis* for stretched PET/TiO_2 fiber at DR = 1.3

Test microorganism	O.D after 24 h. 600 nm		Reduction (Rp) % for PET/TiO_2 fibers at DR = 1.3
	Blank PET fiber	PET/TiO_2 at DR = 1.3	
Bacillus subtilis	0.360	0.030	91.6%

To investigate the variation in refractive indices of treated PET/TiO_2 fibers along its axes, each treated fiber at specific annealed temperature and duration is fixed on a glass slide and immersed in liquid of refractive index 1.65 and then they are transferred to the microscope stage in optical setup of TIE in Fig. 1A. At each annealed temperature and duration, three two-dimensional intensity images for the treated PET/TiO_2 fiber separated via 50 microns from focus at the parallel (ǁ) polarization direction are captured at each position along the fiber. The phase maps of the treated PET/TiO_2 fibers at each position are extracted and their 3D refractive indices are calculated. Figure 12 shows the mean of refractive index at each position along the treated PET/TiO_2 fibers after annealing at 70 °C, 80 °C, 90 °C, 100 °C, 110 °C, and 120 °C for durations of 30 min, 60 min, 90 min, and 120 min. From this figure, it is observed that the thermally treated PET/TiO2 fibers at 80 °C for duration 60 min, and 120 °C for durations 60 min and 120 min have the highest stability for variations in the refractive indices along the fiber axis compared with the other annealing temperatures and their durations. This indicates that the distribution and diffusion of TiO_2 nanoparticles along the fiber axis at these annealing temperatures and durations become more regular and homogeneous compared to untreated samples. To ensure these results, for example, the extracted phase map and its filled contour plot at fiber position $d = 9$ mm for thermally treated PET/TiO_2 at 120 °C for duration 120 min are compared with the extracted phase map and its filled contour plot for untreated PET/TiO_2 as shown in Fig. 13. This figure clarifies that the distribution and diffusion of TiO_2 nanoparticles of the treated fiber have more homogeneous.

The antibacterial activates of the most preferable annealing temperatures and durations for the PET/TiO_2 fiber are evaluated using the shaking flask method as given in Table 3. This table clarifies that the reduction percentages for annealed samples (Rp1 = 86.1%, Rp2 = 88.1%, and Rp3 = 89.7%) are higher than the reduction rate for untreated fiber (Rp = 80.5%) in Table 1. This indicates that the annealing process not only improves the optical properties but also improves the antibacterial activity of fibers. Furthermore, Table 3 illustrates that the annealed fiber at 120 °C for duration 120 min (Rp3) has the higher antibacterial activity compared to the other annealing conditions.

5.6 Influence of the cold drawing process on the optical properties of thermally treated PET/TiO_2 fibers

For selected annealing conditions in above study, opto-mechincal investigations for treated PET/TiO_2 fibers at these temperatures and durations are performed. Here, each single treated fiber is fixed between the clamps of the stretching device unit and immersed in liquid of refractive index 1.65 and then they are transferred to the optical system of TIE technique. Signals are sent to the stepper motor SM_1 to draw each treated PET/TiO_2 fiber at different draw ratios. For each draw ratio, three two-dimensional intensity images for each treated PET/TiO_2 fiber separated via 50 microns from focus at the parallel (ǁ) polarization direction are recorded.

The phase map and the 3D refractive index for each treated fiber at each draw ratio are calculated. Figure 14 shows the relationship between the mean refractive index and draw ratio of treated PET/TiO_2 fibers at annealing temperatures 80 °C for duration 60 min, and 120 °C for durations 60 and 120 min. This figure clarifies that the fracture point for annealed PET/TiO_2 fiber at 80 °C for duration 60 min occurred at draw ratio 1.2, while for annealed PET/TiO_2 fibers at 120 °C for durations 60 and 120 min, the fracture points occurred at draw ratios 1.3 and 1.55, respectively. Also, comparing untreated sample in Fig. 11 that has fracture point at draw ratio 1.35 with treated sample at 120 °C for duration 120 min in Fig. 14, that has fracture point at draw ratio 1.55, one concludes that the annealed PET/TiO_2 fibers at 120 °C for durations 120 min has the most preferable mechanical properties. Furthermore, the

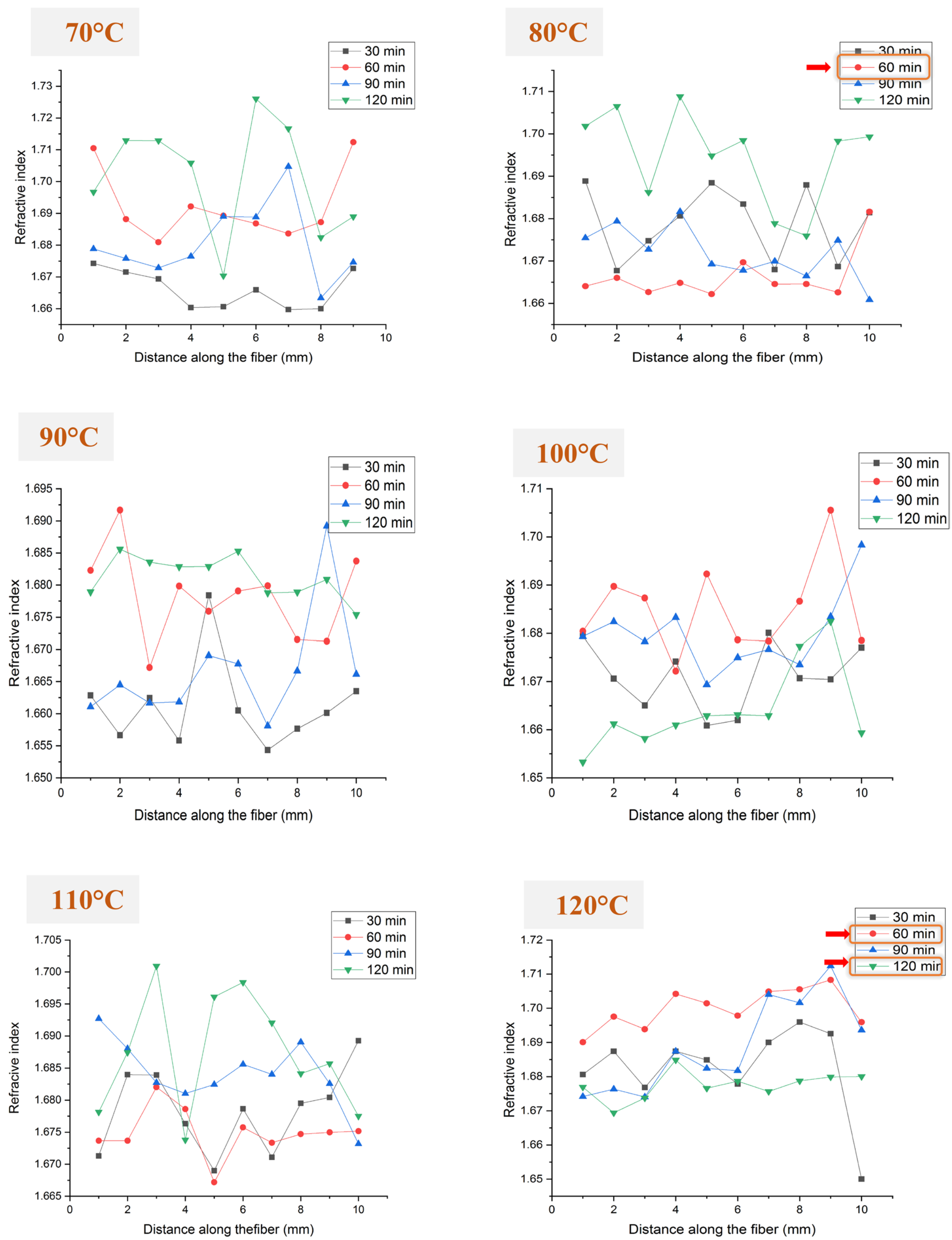

Fig. 12 Relation between the mean refractive index of PET/TiO_2 fiber as a function of fiber position for different annealing conditions

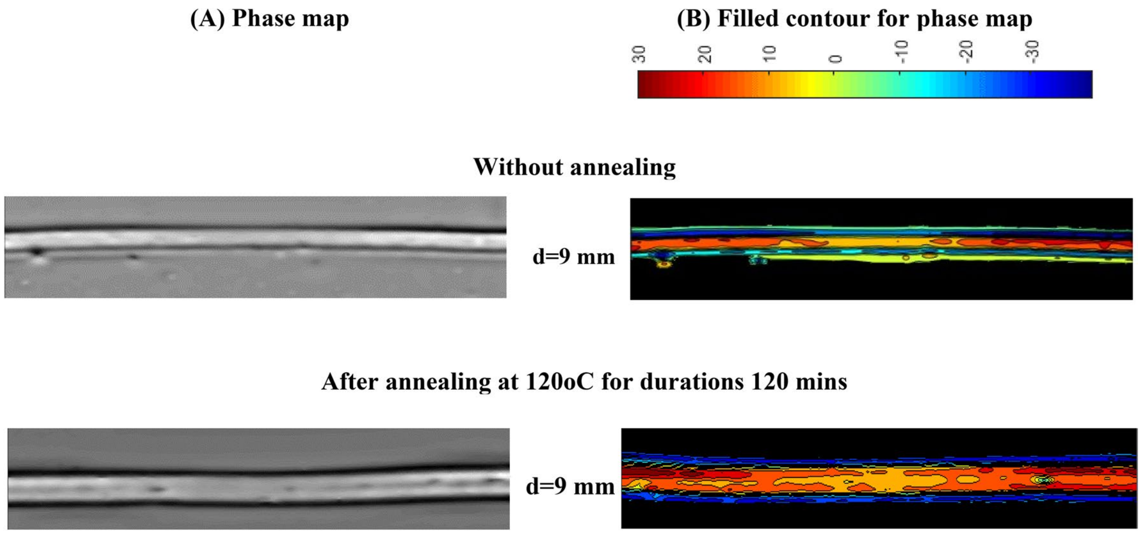

Fig. 13 The phase maps and their filled contour plots for untreated PET/TiO_2 fiber and annealed PET/TiO_2 fiber at 120 °C for duration 120 min for $d = 9$ mm

Table 3 The reduction percentage in the growth of *Bacillus subtilis* for the most preferable annealing temperatures and durations for the PET/TiO_2 fiber

Test microorganism	O.D after 24 h. 600 nm				Reduction (Rp) % for PET/TiO_2 fibers		
	Blank PET fiber	Different annealing conditions for PET/TiO_2 fibers					
		80 °C 60 min	120 °C 60 min	120 °C 120 min	Rp1	Rp2	Rp3
Bacillus subtilis	0.360	0.050	0.043	0.037	86.1%	88.1%	89.7%

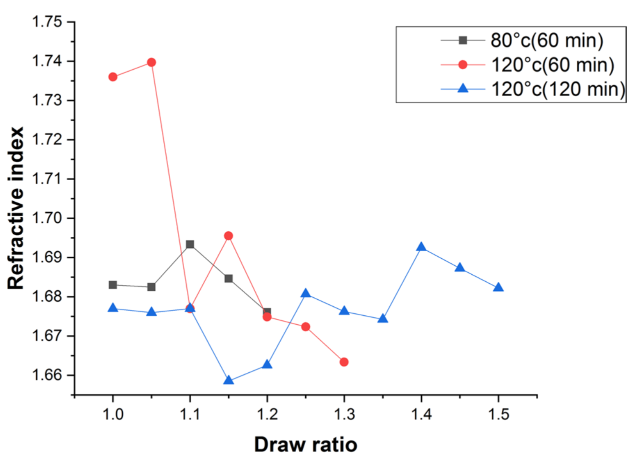

Fig. 14 The relationship between the mean refractive index and draw ratio of treated PET/TiO_2 fibers at annealing temperatures 80 °C for duration 60 min, and 120 °C for durations 60 and 120 min

trend of the refractive index for annealed PET/TiO_2 fibers at 120 °C for durations 120 min at each draw ratio is improved compared to the trend of the untreated sample in Fig. 11. These improvements in the mechanical and the optical properties can be attributed to increased mobility of the polymer chains at higher annealing temperatures and durations.

The shaking flask method is used to evaluate the antibacterial activates for the most preferable annealing temperatures and durations of the stretched PET/TiO_2 fibers at the draw ratios that precede the fracture process for each sample and the results are given in Table 4. This table clarifies that the drawn fiber at draw ratio 1.45 after annealing at 120 °C for duration 120 min has the higher antimicrobial activity value compared to the drawn fiber without annealing or drawn fibers at other annealing conditions.

Table 4 The reduction percentage in the growth of *Bacillus subtilis* for the most preferable annealing temperatures and durations of the stretched PET/TiO_2 fibers at different draw ratios that precedes the fracture process for each sample

Test microorganism	O.D after 24 h. 600 nm				Reduction(Rp) % for PET/TiO_2 fibers		
	Blank PET fiber	Drawing fiber after annealing for PET/TiO_2 fibers					
		80 °C 60 min DR = 1.15	120 °C 60 min DR = 1.25	120 °C 120 min DR = 1.45	Rp1	Rp2	Rp3
Bacillus subtilis	0.360	0.041	0.032	0.019	88.6%	91.1%	94.7%

6 Conclusions

The effect of stretching and annealing conditions on the optical, mechanical features, and antibacterial activity of PET/TiO_2 fibers are investigated via the TIE technique. The variation of the refractive index of untreated PET/TiO_2 fiber along its axis is studied. The TIE technique is used to carry out investigation for the variations in the refractive index due to the stretching. The antimicrobial activity of the PET/TiO_2 fibers are evaluated before and after stretching. The influence of annealing on the variation of the refractive index of PET/TiO_2 fiber along its axis and the distribution of TiO_2 are investigated. The results showed that the thermally treated PET/TiO_2 fibers at 80 °C for duration 60 min, and 120 °C for durations 60 min and 120 min have the highest stability for variations in the refractive indices and highest homogeneity for distribution TiO_2 along the fiber axis. The treated PET/TiO_2 fibers at these temperatures and durations are stretched at different draw ratios. Upon stretching at these annealing conditions, it is found that the stretched PET/TiO_2 fibers at 120 °C for duration 120 min have the most preferable optical, mechanical, and antimicrobial properties.

Acknowledgements We would like to express our deep thanks to Prof. Dr S. E. Shalaby (Textile Research Division, National Research Center, Dokki, Cairo, Egypt) for preparing and providing PET/TiO_2 samples.

References

1. H.M. Hafez, Y.A. Attia, Challenges to the poultry industry, current perspectives and strategic future after the COVID-19 outbreak. Front. Vet. Sci. **7**, 516 (2020)
2. J. Sharifi-Rad, C.F. Rodrigues, Z. Stojanović-Radić, M. Dimitrijević, A. Aleksić, K. Neffe-Skocińska, D. Zielińska, D. Kołożyn-Krajewska, B. Salehi, S. Milton Prabu, F. Schutz, Probiotics: versatile bioactive components in promoting human health. Medicina (Lithuania) **56**, 433–463 (2020)
3. N.G. Al-Balakocy, S.E. Shalaby, Imparting antimicrobial properties to polyester and polyamide fibers-state of the art. J. Text. Assoc. **78**, 179–201 (2017)
4. R.K. Matharu, Z. Charani, L. Ciric, U.E. Illangakoon, M. Edirisinghe, Antimicrobial activity of tellurium-loaded polymeric fiber meshes. J. Appl. Polym. Sci. **135**, 46368 (2018)
5. E. Kenawy, S.D. Worley, R. Broughton, The chemistry and applications of antimicrobial polymers: a state-of-the-art review. Biomacromol **8**, 1359–1384 (2007)
6. A.K. Yetisen, H. Qu, A. Manbachi, H. Butt, M.R. Dokmeci, J.P. Hinestroza, M. Skorobogatiy, A. Khademhosseini, S.H. Yun, Nanotechnology in textiles. ACS Nano **10**, 3042–3068 (2016)
7. Y.N. Slavin, J. Asnis, U.O. Häfeli, H. Bach, Metal nanoparticles: understanding the mechanisms behind antibacterial activity. J. Nanobiotechnol. **15**, 1–20 (2017)
8. O. Bshena, T.D.J. Heunis, L.M. Dicks, B. Klumperman, Antimicrobial fibers: therapeutic possibilities and recent advances. Future Med. Chem. **3**, 1821–1847 (2011)
9. M.R. Teague, Deterministic phase retrieval: a green's function solution. JOSA **73**, 1434–1441 (1983)
10. T.Z. Sokkar, K.A. El-Farahaty, M.A. El-Bakary, M.I. Raslan, E.Z. Omar, A.A. Hamza, Non-interferometric determination of optical anisotropy in highly-oriented fibres using transport intensity equation technique. Opt. Lasers Eng. **102**, 10–16 (2018)
11. E.Z. Omar, M.A. El-Bakary, A suggested optical setup for duplicated-image transport intensity equation technique to accurate determine the optical anisotropy in fibers. Optik **245**, 16773 (2021)
12. E.Z. Omar, M.A. El-Bakary, An immersion microscopy method for determining the optical anisotropy in fibres using transport intensity equation technique. Appl. Phys. B Lasers Opt. **125**, 1–12 (2019)
13. E.Z. Omar, Investigation and classification of fibre deformation using interferometric and machine learning techniques. Appl. Phys. B Lasers Opt. **126**, 1–14 (2020)
14. L. Waller, L. Tian, G. Barbastathis, Transport of intensity imaging with higher order derivatives. Opt. Express **18**, 12552 (2009)
15. T.Z.N. Sokkar, K.A. El-farahaty, M.I. Raslan, A.A. Hamza, Experimental investigation of craze morphology of isotactic polypropylene using computed tomography. J. Microsc. **263**, 97–105 (2016)
16. T.Z.N. Sokkar, K.A. El-Farahaty, W.A. Ramadan, H.H. Wahba, M.I. Raslan, A.A. Hamza, Nonray-tracing determination of the 3D refractive index profile of polymeric fibres using single-frame computed tomography and digital holographic interferometric technique. J. Microsc. **257**, 208–216 (2015)
17. R.A. Geise, Computed tomography: physical principles, clinical applications, and quality control. Radiology **194**, 782–782 (1995)
18. N. Bevins, J. Zambelli, K. Li, Z. Qi, G.H. Chen, Multicontrast x-ray computed tomography imaging using Talbot-Lau interferometry without phase stepping. Med. Phys. **39**, 424–428 (2012)
19. T.Z.N. Sokkar, K.A. El-Farahaty, E.A. Seisa, E.Z. Omar, M. Agour, Online investigation of optical properties and craze propagation of drawn polypropylene fiber by using interferometric image analysis. Opt. Photonics J. **4**, 165–181 (2014)
20. T.Z.N. Sokkar, K.A. El-Farahaty, F.E. Hanash, E.Z. Omar, In situ investigation of the effect of stretching speed and annealing conditions on the crazing of as-spun IPP fibres using Pluta polarizing interference microscope. Optik **127**, 102–106 (2016)

21. E.Z. Omar, T.Z.N. Sokkar, A.A. Hamza, In situ investigation and detection of opto-mechanical properties of polymeric fibres from their digital distorted microinterferograms using machine learning algorithms. Opt. Laser Technol. **129**, 106295 (2020)
22. T.Z.N. Sokkar, K.A. El-Farahaty, H.M. El-Dessouky, F.E. Hanash, Optical and structural properties of thermally treated iPP fibers: effect of strain rate. Opt. Lasers Eng. **51**, 542–552 (2013)
23. E.Z. Omar, A computational phase-shifting interferometric method using a single-shot microinterferogram and its application. Optik **217**, 164294 (2020)
24. S.E. Shalaby, M.A. Saad, N.G. Al-Balakocy, A.-E.O. Srm, M.K. Beliakova, Physical fixation of antimicrobial substances (AS) into polyester fibers manufactured from recycled chips. Int. J. Appl. Chem. **11**, 121–133 (2015)
25. J.W. Liou, H.H. Chang, Bactericidal effects and mechanisms of visible light-responsive titanium dioxide photocatalysts on pathogenic bacteria. Arch. Immunol. Ther. Exp. (Warsz) **60**, 267–275 (2012)
26. S.M. Dizaj, F. Lotfipour, M. Barzegar-Jalali, M.H. Zarrintan, K. Adibkia, Antimicrobial activity of the metals and metal oxide nanoparticles. Mater. Sci. Eng. C **44**, 278–284 (2014)
27. M. Azizi-Lalabadi, A. Ehsani, B. Divband, M. Alizadeh-Sani, Antimicrobial activity of titanium dioxide and zinc oxide nanoparticles supported in 4A zeolite and evaluation the morphological characteristic. Sci. Rep. **9**, 1–10 (2019)
28. F.E. Al-Tahhan, A.A. Sakr, D.A. Aladle, M.E. Fares, Improved image segmentation algorithms for detecting types of acute lymphatic leukaemia. IET Image Process. **13**, 2595–2603 (2019)
29. P. Tao, Y. Li, A. Rungta, A. Viswanath, J. Gao, B.C. Benicewicz, R.W. Siegel, L.S. Schadler, TiO2 nanocomposites with high refractive index and transparency. J. Mater. Chem. **21**, 18623 (2011)
30. T.Z.N. Sokkar, M.A. El-Bakary, M.I. Raslan, N.A. Al-Kalali, E.Z. Omar, Dynamic investigations of opto-mechanical properties of iPP/TiO_2 nanocomposites fbres using fringe analysis techniques. Optik **212**, 164683 (2020)
31. M. Takafuji, M. Kajiwara, N. Hano, Y. Kuwahara, H. Ihara, Preparation of high refractive index composite films based on titanium oxide nanoparticles hybridized hydrophilic polymers. Nanomaterials **9**, 514 (2019)
32. M. Vermillac, H. Fneich, J. Turlier, M. Cabié, C. Kucera, D. Borschneck, F. Peters, P. Vennéguès, T. Neisius, S. Chaussedent, D.R. Neuville, A. Mehdi, J. Ballato, W. Blanc, On the morphologies of oxides particles in optical fibers: effect of the drawing tension and composition. Opt. Mater. **87**, 74–79 (2019)
33. S. Haq, W. Rehman, M. Waseem, R. Javed, M. Ur-Rehman, M. Shahid, Effect of heating on the structural and optical properties of TiO2 nanoparticles: antibacterial activity. Appl. Nanosci. **8**, 11–18 (2018)